P-07-14

Reduction of fracture slip due to shielding effect from surrounding fractures

Billy Fälth, Harald Hökmark
Clay Technology AB

January 2007

Svensk Kärnbränslehantering AB
Swedish Nuclear Fuel
and Waste Management Co
Box 5864
SE-102 40 Stockholm Sweden
Tel 08-459 84 00
+46 8 459 84 00
Fax 08-661 57 19
+46 8 661 57 19

ISSN 1651-4416
SKB P-07-14

Reduction of fracture slip due to shielding effect from surrounding fractures

Billy Fälth, Harald Hökmark
Clay Technology AB

January 2007

Contents

1 Introduction

The KBS-3 repository concept for storage of high level radioactive wastes is based on horizontal tunnels at 400–700 m depth in crystalline rock. The wastes will be deposited in copper canisters which are placed in vertical deposition holes in the tunnel floor and surrounded by a low-permeability, flexible barrier of highly compacted bentonite. The surrounding bedrock is together with the canister and the bentonite forming a barrier system, which aims at preventing radio nuclides from reaching the biosphere at the ground surface. The spent fuel will be dangerous for hundreds of thousands of years and it is important for the repository safety that the barrier system sealing properties are stable over long times.

According to the long time perspectives, the safety assessments include the possibility of future seismic activity and its implications for the repository safety. A seismic event close to the repository may cause slip along rock fractures inside the repository. A particular concern is the possibility of seismically induced slip on fractures intersecting deposition holes. If the slip along such a fracture is sufficiently large, it could possibly cause damage of the canister. According to the present-day canister damage criterion applied by SKB, the slip on a fracture intersecting a deposition hole must not exceed 100 mm /Hedin 2005/.

The question is raised if seismically induced fracture slip can be reduced by the presence of larger surrounding fractures. The idea is that the surrounding fractures form a shield that accomodate shear movements during a seismic event and thus limit the shear stresses in the fracture of interest. Previous 2D modeling work has indicated that this process may take place /Hökmark 1992/. In Figure 1-1, results from UDEC calculations are shown. The left picture shows the fracture geometry and history point locations. The loading of the model was done as a step-wise rotation of the stress field. The development of shear displacements are shown in the diagram (right). The angles indicate the step-wise rotation of the stress field. When the fracture slip at the points 3, 4 and 5 are compared, it becomes clear that the amount of slip at point 4 is reduced due to the location of this point in a region which is completely enclosed by other fractures. A similar reduction at point 9 can be observed when the amount of slip at this point is compared to the displacements at point 8 and 10. The main objective of the present study was to evaluate the shielding effect when expanding the study of /Hökmark 1992/ into 3D.

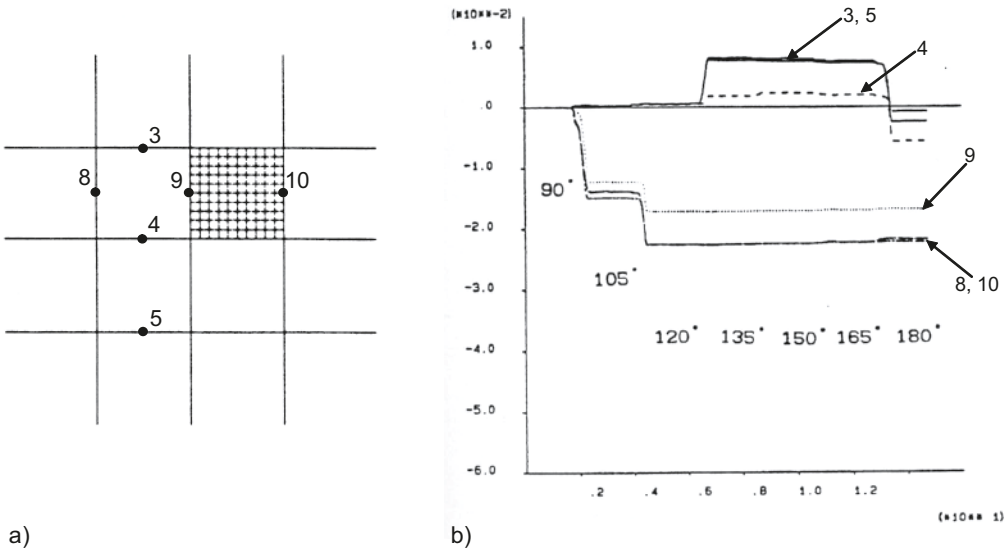

Figure 1-1. *Reduction of fracture shear displacement due to the presence of surrounding fractures. a) Fracture geometry and history point locations, b) fracture shear displacement. Results obtained from previous UDEC analyses /Hökmark 1992/.*

2 Objectives

The main objective of this work was to examine if slip on a shielded fracture (target fracture), caused by stress changes in the rock mass, could be reduced by the presence of surrounding fractures (shielding fractures). The work has been carried out by static analyses of numerical models in which a target fracture and a number of shielding fractures were included. The models were analyzed by use of 3DEC, which is a three-dimensional program based on the distinct element method /Itasca 2003/. Embedded within 3DEC, there is a programming language called FISH, which enables the user to define new variables and functions that may be used to add user-defined features to the code. FISH was used here for the development of a technique for defining circular fractures with certain radii, orientations and properties.

3 Description of 3DEC models

3.1 General

The models were analyzed by use of 3DEC (3-Dimensional Distinct Element Code) which is a computer program for discontinuum modeling based on the distinct element method. 3DEC simulates the response of discontinuous media (such as a jointed rock mass) subjected to either static or dynamic loading. The discontinuous medium is represented by an assemblage of discrete blocks /Itasca 2003/.

To facilitate the understanding of the text, the following definitions are made:

1. *Target fracture:* The fracture that potentially is reactivated by stress changes in the rock mass. The maximum slip on this fracture is the main result of this study.
2. *Shielding fractures:* Fractures that surround the target fracture. The shielding effect from these fractures is to be examined in the work.

Two models were analyzed: Model A and Model B. The models had the same outer dimensions, in situ stresses, boundary conditions and material properties. The difference between the models regards the following:

- *Model A*: This model was set up to demonstrate the effect of shielding fractures that completely encloses a target fracture. The orientations of the shielding fractures in the model were set to maximize their influence on the shear displacement of the target fracture.
- *Model B*: The shielding fracture geometries in this model were provided by a realization of the Discrete Fracture Network (DFN) model for the Forsmark site, version 1.2 /SKB 2005b/.

3.2 Outline of model geometry

The outline of the model geometry, initial conditions and boundary conditions are the same for both Model A and Model B. The outlines of the models are shown in Figure 3-1. The models consist of a box with the dimensions 5,000·2,000·5,000 metres (x·y·z) and with the model top representing the ground surface. The origin is located at the model center. Note that a left-handed coordinate system is used in 3DEC.

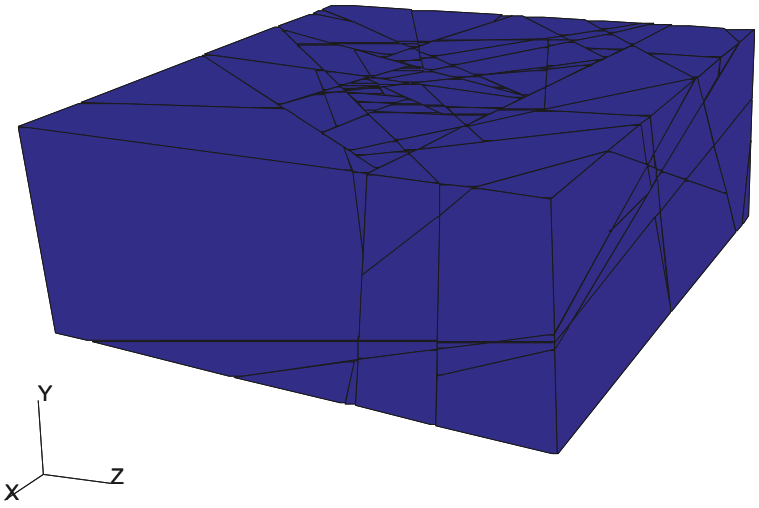

Figure 3-1. *Outline of model geometry.*

3.3 Initial conditions

The initial stress state is shown in Figure 3-2. The stress was assumed to vary with depth. The higher in situ stress at great depths gives the shielding fractures higher strength which will reduce their shielding effect. Thus this is judged to be conservative compared to a case where the in situ stress is constant with depth. The gravitational acceleration in the negative y-direction was set to 9.81 m/s^2.

3.4 Load sequence and boundary conditions

The analyses were divided into three steps (Figure 3-3):

1. The in situ stresses were incorporated and static equilibrium was achieved.
2. One of the vertical boundaries was moved 3.6 metres in the negative z-direction. The amount of boundary displacement was calibrated to give 0.1 metre slip on the target fracture with no shielding fractures active (Case 1, cf Section 3.8).
3. Static equilibrium was achieved.

The bottom of the models and all vertical boundaries had roller boundaries. The upper boundary was free.

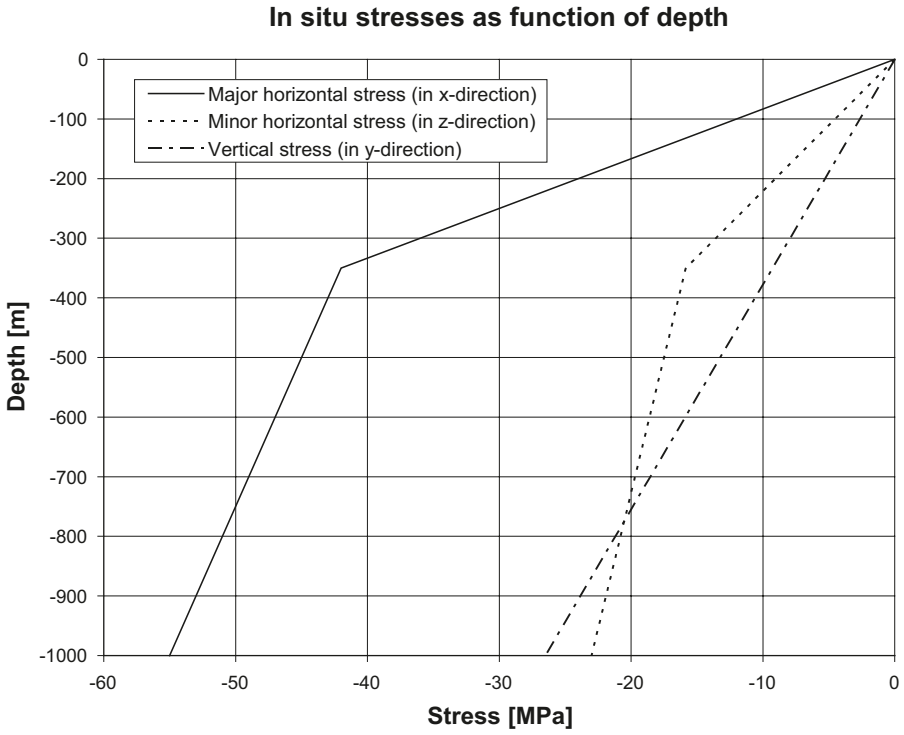

Figure 3-2. *Initial stresses as function of depth.*

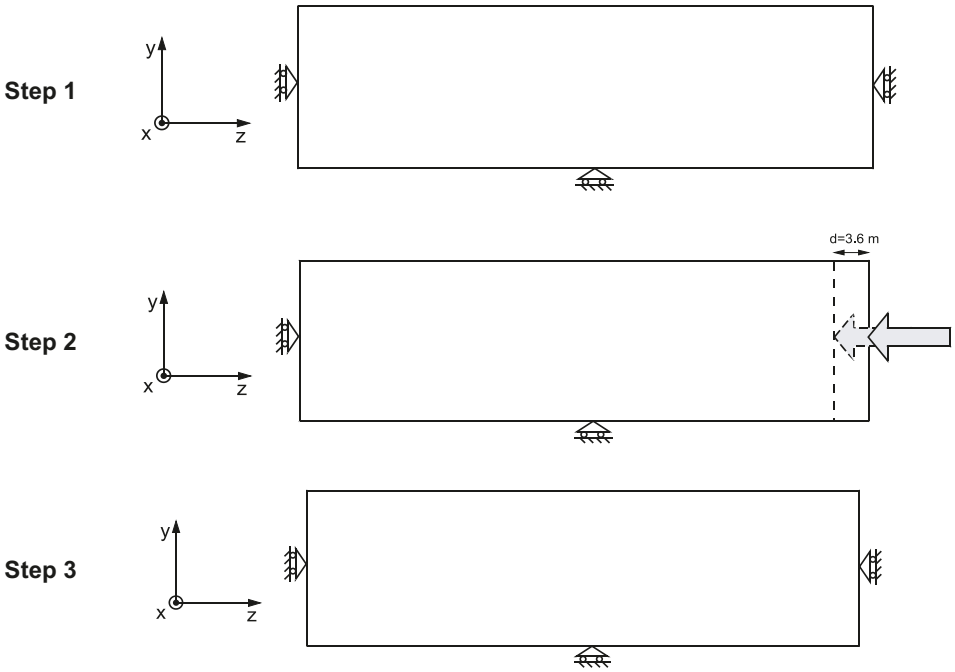

Figure 3-3. *Load sequence scheme and boundary conditions.*

3.5 Fracture system geometry

3.5.1 General

Two types of models were analyzed. The difference between the models regards the shape of the shielding fracture system. The shielding fractures in Model A were set up to form an idealized fracture box. In Model B, the shielding fracture system was based on a DFN realization. In both models, the target fracture was circular with a radius of 100 m and was located 500 m below ground surface. Its dip- and dip direction angles were 45° and 180°, respectively (see Figure 3-7 for explanation of the meaning of dip-and dip direction in 3DEC.)

3.5.2 Model A: Shielding fracture box

The shielding fractures in Model A were set up to form a box that completely enclosed the target fracture. In Figure 3-4, the fracture geometry is shown. The shielding fractures (marked with dark blue) had a dip angle of 45° and the box that was formed was quadratic with an edge length of 424 m. However, the shielding fractures extended outside the quadratic box and reached top and bottom of the model. The shielding fracture orientation was chosen to obtain high shear stresses in the shielding fractures with large shielding fracture slip as a consequence. The idea is that large slip in the shielding fractures prevents the deviatoric stresses from the surrounding rock mass to be transferred into the box. The reduction of the deviatoric stresses inside the box reduces the slip on the target fracture.

3.5.3 Model B: Shielding fracture geometries according to DFN model

In Model B, the shielding fracture geometries were taken from a realization of the Discrete Fracture Network (DFN) model for Forsmark, version 1.2 /SKB 2005b/. The volume used in the realization had the dimensions 15,000·11,000·2,200 metres and contained 3,160 fractures with radii spanning from 250 to 1,000 metres. The 3DEC model had significantly smaller dimensions compared to that of the DFN realization volume. Thus, a limited number of fractures where chosen to be incorporated into the 3DEC model. This was done in two steps:

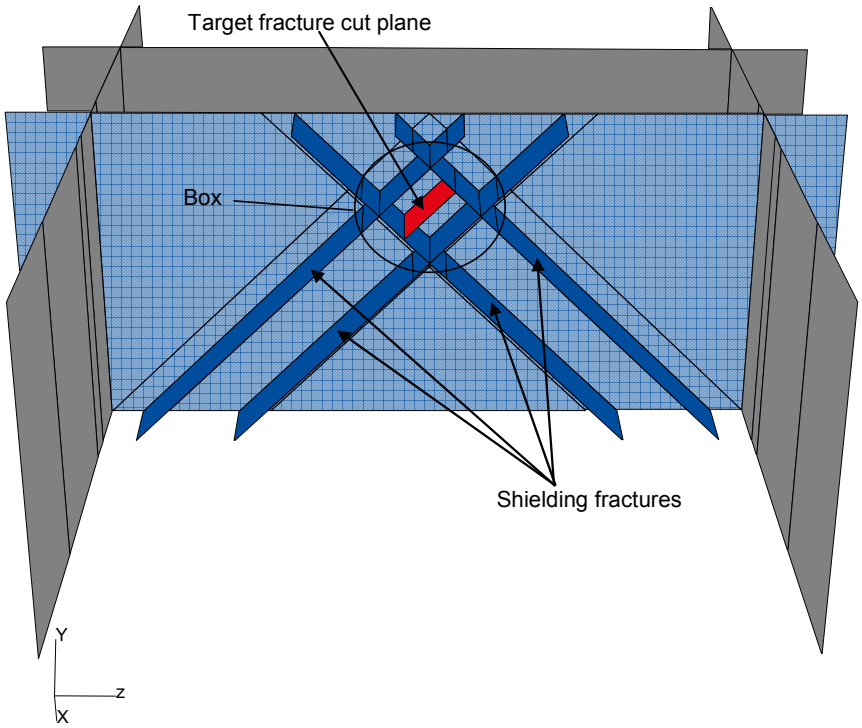

Figure 3-4. *Shielding fracture box geometry in Model A. The shielding fractures (dark blue) extended to top and bottom of model. One vertical shielding fracture plane is hidden to show the geometry of the box.*

Step 1:

Fractures fulfilling the following criteria were selected:

- Fractures, with edges located within –1,000 < y < 1,000 m.
- Fractures with centers located within –1,500 < x, z < 1,500 m.

Step 2:

In this step, the orientations of the fractures selected in step one were considered. The Mohr-Coulomb criterion for failure was used to select fractures with orientations which are favorable for slip during loading of the model. The loading of the model was done parallel to the z-axis. Thus, inclined fractures oriented such that their dip directions β (cf Figure 3-7) are close to 0° or 180° (parallel with z-axis) will be subjected to high shear stress changes during loading. The effect on these fractures of the loading is illustrated with Mohr's circle of stress in Figure 3-5 (bottom). In the figure, the failure envelopes for fractures with friction angles of 20° and 30° also are plotted. Two states of stress at 500 m depth for these fractures are shown:

1. *Initial state:* The first state is the in situ stress state when the intermediate principal stress $\sigma_2 = \sigma_z$ is 17.5 MPa and the minor principal stress $\sigma_3 = \sigma_y$ is 13.25 MPa. The maximum shear stress in this state is well below the failure envelope for both friction angles 20° and 30°.
2. *Loaded state:* After the loading, σ_z has increased to ~ 69 MPa and both failure envelopes are crossed.

The shaded region indicates the part of the semi circle in the second stress state that lies above the 30° failure envelope. The circle sector that corresponds to this area is defined by θ_1–θ_2. This means that a fracture with friction a angle of 30° and with dip direction β of 0° or 180° (parallel with z-axis) will slip if its dip angle α fulfills

$$\frac{\theta_2}{2} \leq \alpha \leq \frac{\theta_1}{2} \qquad (1)$$

This was used as a guideline when shielding fractures were selected. Since there were uncertainties about how many fractures which was possible to handle in the model, dip angles within the interval (1) where selected in the first place. When Figure 3-5 is studied, it also becomes clear that if the fractures have lower strength (e.g. friction angle 20°), the angle interval (1) will be larger and a larger number of fractures are likely to slip.

The orientations of the shielding fractures are illustrated in Figure 3-6. The fractures are defined by their center coordinates, radii, dip- and dip direction angles. Figure 3-7 shows how the dip- and dip directions are related to the 3DEC coordinate system. The dip angle α is positive down from the horizontal (x-z) plane and the dip direction β is the angle clock-wise from the z-axis.

The horizontal location (x- and z-coordinates) of the target fracture was chosen such that intersection with shielding fractures was avoided. The dip direction was 180° and the dip angle was 45°. The rock volume in which the target fracture was located is shown in Figure 3-8. The boundaries of this volume were settled by a number of the shielding fracture cut planes. In three of the cases analyzed, all of the surfaces defining this rock volume were used as shielding fractures. This was done in order to examine the effect of using this rock part as a completely enclosing shielding fracture box in analogy with the box in Model A.

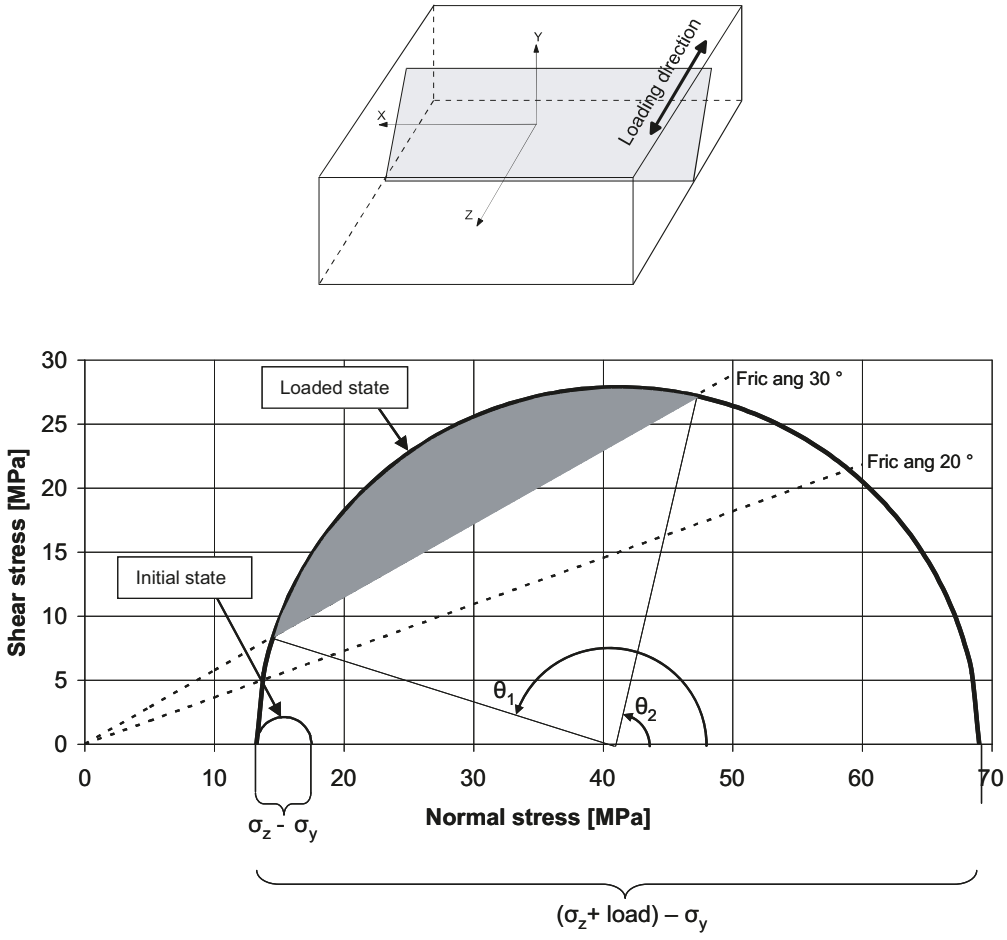

Figure 3-5. *Top: Orientation of fractures with dip directions parallel with the z-axis (dip directions 0° and 180°). Bottom: Mohr's circle diagram.*

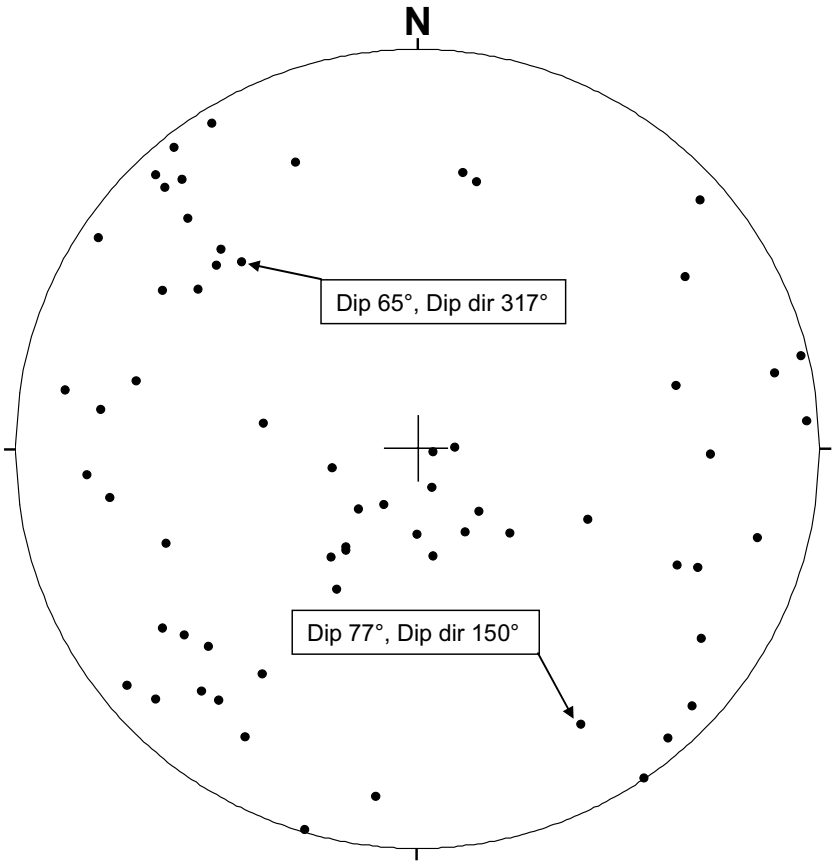

Figure 3-6. *Stereonet showing the shielding fracture orientations in Model B. Two fractures are labeled to illustrate sense of Dip and Dip Direction.*

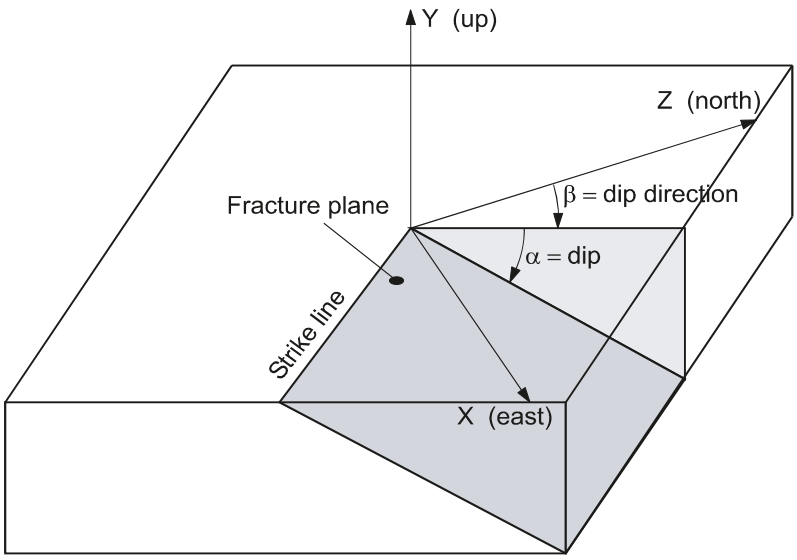

Figure 3-7. *The figure shows how dip- and dip direction relate to the coordinate system in 3DEC. Note that 3DEC uses a left-handed coordinate system.*

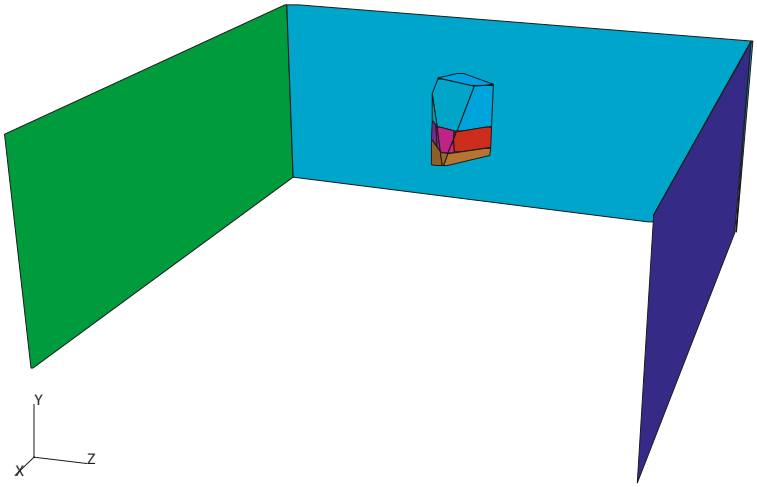

Figure 3-8. *Rock volume in which the target fracture was located in Model B.*

3.6 Technique for definition of circular fractures

In 3DEC, models are built of rock blocks that can be either rigid or deformable. Between the blocks, discrete cut planes are defined. Within these planes there is a contact logic that controls the mechanical interaction between the blocks. The logic detects if blocks are losing contact or if blocks find new contact points. The normal- and shear forces as well as normal- and shear displacements between the blocks are calculated. A cut plane can only be created by complete division of a block and the cut plane shape is defined by the shape of the divided block. This is illustrated in Figure 3-9, which is a plot of all 3DEC cut planes in Model B.

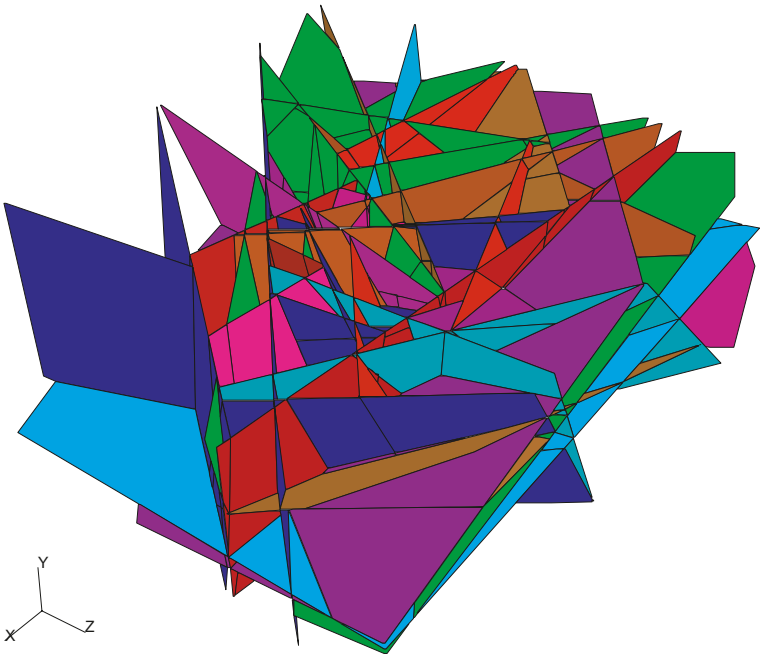

Figure 3-9. *Shielding fracture cut planes in Model B. In 3DEC, the shapes of the cut planes are settled by the shape of the divided blocks.*

In this study circular fractures where used. Thus, only parts of the cut planes were used as active fracture areas. This could be done by the use of a FISH routine. The principle used for this procedure is illustrated in Figure 3-10. A fracture was defined as the circular area created by the intersection between two geometric entities:

1. A sphere with its center located in the center of the fracture and with its radius equal to that of the fracture.
2. A 3DEC cut plane intersecting the center point of the sphere and with intended dip and dip direction angles.

This circular area was assigned with fracture properties. The remaining area of the cut plane was assigned with fictitious fracture properties that prevented slip.

3.7 Material properties

The rock was assumed to be linearly elastic. For the fractures, the Mohr-Coulomb failure model was used. The target fracture was assumed to be frictionless. This is a conservative assumption which was made to account for the possibility of normal stress loss with accompanying fracture shear strength loss due to dynamic effects during a seismic event. The material property parameter values are presented in Table 3-1. The elastic parameter values of the rock mass and of the fractures were obtained from the Forsmark Site Descriptive Model, version 1.2 /SKB 2005b/.

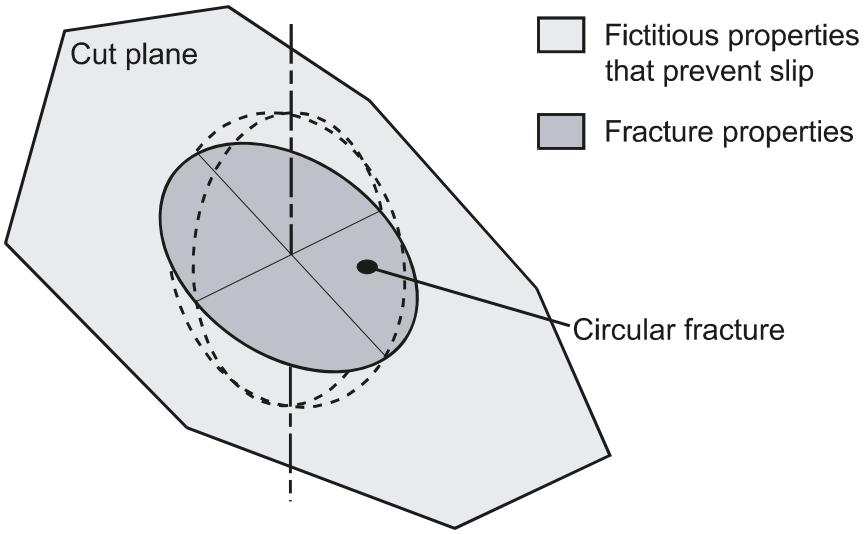

Figure 3-10. *The principle used for defining circular fractures from arbitrary polygon shaped 3DEC cut planes. The circular fracture was defined as the intersection between a sphere and the cut plane.*

Table 3-1. Material property parameter values.

Component	3DEC parameter	Unit	Value	Note
Rock mass	Density	kg/m^3	2,700	1
	Young's modulus	GPa	68	1
	Poisson's ratio	–	0.22	1
Shielding fractures	Joint normal stiffness	GPa/m	128	1
	Joint shear stiffness,	GPa/m	39	1
	Friction angle	deg	30, 25, 20, 15, 10, 0	2
Target fracture	Joint normal stiffness	GPa/m	128	1
	Joint shear stiffness,	GPa/m	39	1
	Friction angle	deg	0	3

1) According to Forsmark SDM, ver. 1.2 /SKB 2005b/.

2) Different values used. The highest value of 30 degrees is of about the same magnitude as reported for rock fractures in Forsmark SDM, ver. 1.2 /SKB 2005b/.

3) Friction set to zero to account for possible fracture normal stress loss with accompanying shear strength loss due to dynamic effects during a seismic event.

3.8 Case overview

In Table 3-2, a list of all cases that were analyzed is presented. Case 1 is a reference case where no shielding fractures were active. This case was used to calibrate the boundary loading (cf Figure 3-3) to give a maximum shear displacement in the target fracture of 100 mm. The same loading was then used in all cases. Model A includes Case 2–Case 3. The difference between Case 2 and Case 3 regards the shielding fracture friction angle.

Case 4 through Case 14 were based on Model B. Parameters that have been varied are shielding fracture size and shielding fracture friction angle. In Case 4–Case 6, the shielding fractures have radii according to the DFN model realization (i.e. nominal values), whereas in Case 7–Case 14, the shielding fracture radii were doubled. Four values of the shielding fracture friction angle were tried. In addition, in Case 10–Case 14, all of the cut plane surfaces enclosing the rock volume in which the target fracture was located (cf Figure 3-8), were given shielding fracture mechanical properties.

Table 3-2. List of cases that were analyzed.

Model	Case	Shielding fractures friction angle	Shielding fractures radii	Comment
	1	–	–	Reference case – no shielding fractures
A	2	30	–	“Optimized” fracture box
	3	20	–	“Optimized” fracture box
B	4	30	nominal (according to DFN model)	DFN model
	5	25	nominal	DFN model
	6	20	nominal	DFN model
	7	30	2* nominal	DFN model
	8	25	2* nominal	DFN model
	9	20	2* nominal	DFN model
	10	30	2* nominal	DFN model *)
	11	20	2* nominal	DFN model *)
	12	15	2* nominal	DFN model *)
	13	10	2* nominal	DFN model *)
	14	0	2* nominal	DFN model *)

*) Shielding fracture mechanical properties set in all cut plane surfaces enclosing the rock volume where the target fracture is located (cf Figure 3-8).

4 Results and conclusions

A number of cases have been analyzed. Different geometries and mechanical properties of the shielding fractures have been tried to examine how strong idealizations one needs to make to get any significant shielding effect. Reductions of the shielding fracture friction angle have been done in order to study the sensitivity of the target fracture shear slip to the shielding fracture properties. The following cases were analyzed:

- *Case 1*: Reference case where no shielding fractures were included, i.e. the model behaves elastically and the target fracture shear displacement is maximized (100 mm).
- *Case 2–Case 3*: Idealized shield fracture box enclosing the target fracture (cf Figure 3-4).
- *Case 4–Case 6*: Shielding fracture geometries were taken from DFN model realization (cf Figure 3-6 and Appendix).
- *Case 7–Case 9*: Shielding fracture geometries were taken from DFN model realization. Doubled radii in all shielding fractures.
- *Case 10–Case 14*: Shielding fracture geometries were taken from DFN model realization. Doubled radii in all shielding fractures. All of the cut plane surfaces enclosing the target fracture volume (cf Figure 3-8) have shielding fracture properties.

Modeling results, shown in Figure 4-1, indicate that the target fracture has to be completely enclosed by shielding fractures if any significant reduction of its shear displacement should take place. In Case 2 and Case 3, the effect of the idealized shielding fracture box is clear. In these two cases the box was completely tight and the shielding fractures were oriented to effectively

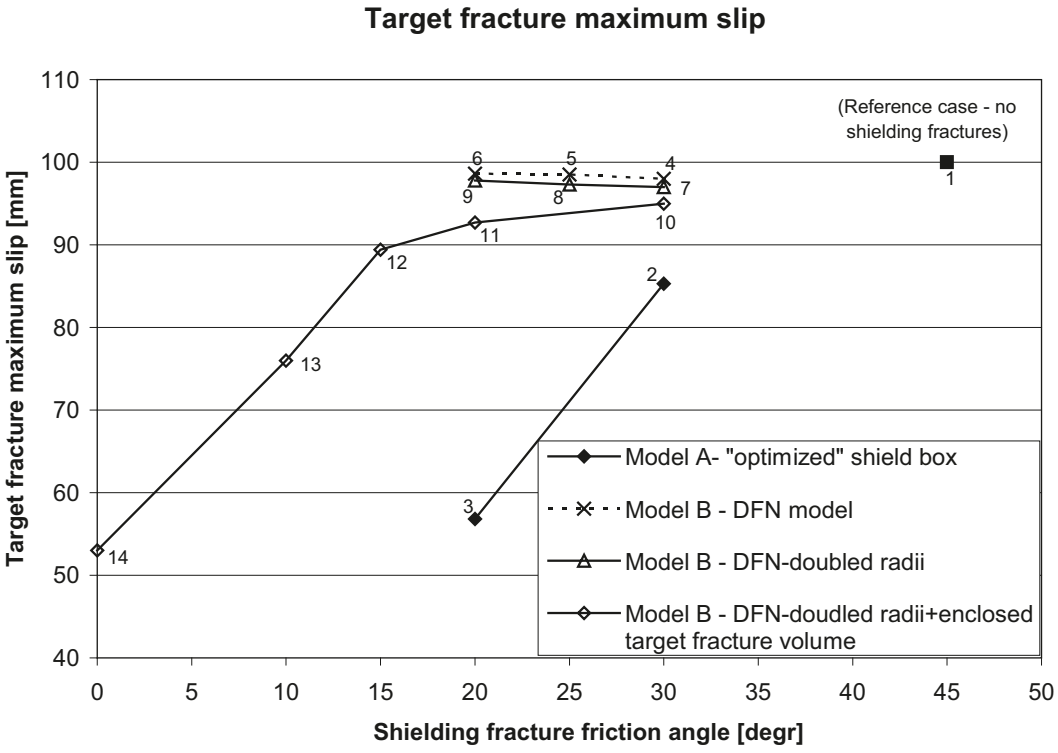

Figure 4-1. *Results from all cases. Case 2–3: Model A with "optimized" shielding fracture box. Case 4–6: Model B with shielding fracture sizes according to DFN model. Case 7–9: Same as Case 4–6 but with doubled shielding fracture radii. Case 10–14: Doubled shielding fractures radii and target fracture volume completely enclosed by shield fractures.*

prevent deviatoric stresses to be transferred into the box. The idealized shielding fracture geometry gives a shielding effect comparable to that of the 2D analyses which are referred to in Figure 1-1. It can be concluded that Case 2 and Case 3 are strongly idealized and it is unlikely to find such combinations of fracture orientations and locations in nature.

In Case 4–Case 6, the shielding fracture geometries were taken from the DFN model realization. The results show no reduction of the target fracture shear displacement. The shielding fracture population contains few fractures with dip angles in the interval 30–60°. Figure 4-2 shows the cumulative frequency of dip angles both in the complete DFN realization and in the fracture population selected to be used in Model B. As can be observed, the share of steeply dipping fractures is significantly larger than that of less steeply oriented fractures. A mix of both steeply and more flattened oriented fractures would increase the likelihood that tight fracture boxes giving shielding effects are formed.

As also can be observed in Figure 4-1, the effect of doubling the shielding fractures radii is negligible (Case 7–Case 9). Even if the radius increase gives an increase of the fracture area by a factor four, it is not enough. In fact, the reduction of shielding fracture friction angle in Case 4–Case 9 causes some increased target fracture slip. This is probably an artifact due to stress concentrations around shielding fracture edges which influences the stress field in the vicinity of the target fracture.

To gain any significant shielding effect in Model B, a strong idealization had to be used. This was done in Case 10–Case 14. Just like in Case 7–Case 9, the shielding fracture diameters were doubled. Besides, the complete cut plane surfaces enclosing the target fracture (cf Figure 3-8) were all given shielding fracture properties. A limited reduction of the target fracture slip was achieved when the friction angle was reduced from 30° to 20°. However, to gain any significant reduction of the target fracture slip, yet more reductions of the shielding fracture friction angle had to be done.

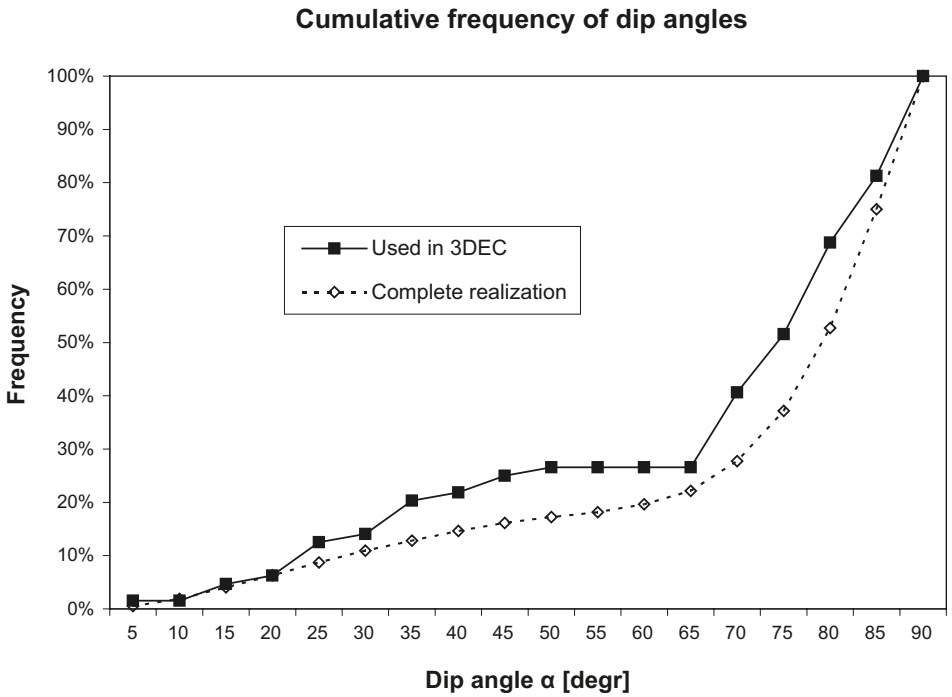

Figure 4-2. *Cumulative frequency of shielding fracture dip angles. Results both for the complete DFN realization and for the fracture population used in Model B are shown.*

It can also be observed that the orientations of the shielding fractures are important for the amount of shielding effect the give. In Case 14, the shielding fractures are frictionless. This gives a reduction of the target fracture slip by about 45%. Almost the same slip reduction is gained in Case 3 where the friction angle is 20°. The main difference between these two cases is that in Case 3 the shielding fracture orientations were optimized to give maximum shielding effect.

The conclusion that can be drawn from the results is that the idealizations regarding shielding fracture geometries and properties have to be driven far to gain any significant reduction of the target fracture shear displacements. The target fracture has to be enclosed by a tight box of shielding fractures with low shear strengths (< 15° friction angle). This type of structures may be found at a large scale in nature. There are evidences of shielding effects in the regional area where the Forsmark candidate site is located. The area is characterized by a relatively high concentration of ductile high-strain zones, which anastomose around tectonic lenses with in general lower strains. During the regional geological evolution, transpressive strains were absorbed by displacements along these ductile deformation zones /SKB 2005b/. However, during the present day conditions and at a smaller scale, the fracture strengths correspond to friction angles of the order of 30° /SKB 2005ab/. Considering the distribution of fracture orientations given by the DFN model used here, the likelihood that a fracture of the same size as the target fracture studied here (about 150 m radius) will be enclosed by a tight box of fractures with low shear strengths (< 15° friction angle) has to be regarded as small.

5 References

Hedin A, 2005. An analytic method for estimating the probability of canister/fracture intersections in a KBS-3 repository. SKB R-05-29. Svensk Kärnbränslehantering AB.

Hökmark H, 1992. Analysis of shear displacements along rock fractures. A preliminary study. SKB Arbetsrapport 92-05. Svensk Kärnbränslehantering AB.

Itasca, 2003. 3DEC – 3 Dimensional Distinct Element Code, User's Guide. Itasca Consulting Group, Inc, Minneapolis.

SKB, 2005a. Preliminary site description. Simpevarp subarea – version 1.2. SKB R-05-08. Svensk Kärnbränslehantering AB.

SKB, 2005b. Preliminary site description. Forsmark area – version 1.2. SKB R-05-18. Svensk Kärnbränslehantering AB.